RESEARCH PROGRESS IN MECHANICAL AND MANUFACTURING ENGINEERING
e-ISSN: 2773-4765

RPMME

Vol. 5 No. 1 (2024) 662-671
https://publisher.uthm.edu.my/periodicals/index.php/rpmme

Aerodynamic Comparison on Different Types of Two-Seater Car Using Ansys CFX

Nur Izzati Zulkarnain[1], Mohammad Kamil Abdullah[1]*

[1] *Faculty of Mechanical and Manufacturing Engineering,*
Universiti Tun Hussein Onn Malaysia, Batu Pahat, Johor, 86400, MALAYSIA

*Corresponding Author: mkamil@uthm.edu.my
DOI: https://doi.org/10.30880/rpmme.2024.05.01.077

Article Info

Received: 30 January 2024
Accepted: 03 June 2024
Available online: 15 September 2024

Keywords

ANSYS, Aerodynamics, Pressure coefficient

Abstract

Two-seater cars are often linked to aerodynamics because of their small size and sporty aesthetics. As these cars are focused on speed, performance, and handling, their design can have a significant impact on their aerodynamic performance. The aim of this study is to evaluate aerodynamic performance on different two-seater cars using ANSYS CFX. The design of the model is derived from the configuration of two-seater cars, featuring a total of four distinct body shapes which are Nissan Skyline, Porsche 918 Spyder, Bugatti Chiron and Ford Mustang. The simulation utilizes element size 0.03mm for all car models, given its lowest percentage difference observed among the tested element sizes. In conclusion, Nissan Skyline, Porsche 918 Spyder and Bugatti Chiron have better aerodynamic efficiency.

1. Introduction

Cars provide convenience, flexibility, and comfort for travel, commuting, and transporting goods. Aerodynamics optimizes how air interacts with a vehicle's body to minimize resistance, increase downforce, regulate airflow for cooling, and reduce turbulence. Streamlined designs with smooth curves significantly decrease air drag, improving fuel efficiency. Two-seaters often feature aerodynamic bodies with sleek shapes.

The Reynolds number is a dimensionless quantity that characterizes the flow pattern of a fluid. It significantly influences the aerodynamics of tested models. Higher Reynolds numbers indicate a greater likelihood of turbulent flow[1]. According to Ananda et al. [2], used Reynolds number to study low Reynolds number aerodynamics in wings with aspect ratios from 2 to 5. Results showed sensitivity to changes in aspect ratio and Reynolds number for all wings. Kumahor & Tachie [3]. employed Reynolds number to examine wake properties, Kelvin-Helmholtz instabilities, and von-Kármán vortex shedding around a rectangular cylinder at moderate Reynolds numbers (3000 to 21000). At low Reynolds numbers (Re < 2100), viscous forces maintain laminar flow, while at high Reynolds numbers (Re > 4000), the flow becomes turbulent with disorganized eddies. Turbulence tendency increases with higher Reynolds Numbers [4].

Luo et al. [5], found that changes in amplitude significantly impact the flow field, while frequency variations do not. Higher amplitude and frequency led to a significant improvement in heat transmission. Weiss et al. [6], investigated hydraulic single-phase mixing in three parallel rectangular channels at different Reynolds numbers and flow regimes. Multi-regime mixing performed better than turbulent mixing due to a more pronounced inner flow velocity drop and a shorter mixing length. Research by Salahuddin et al. [7] shows that introducing nanoparticles to a tangent hyperbolic nanofluid at the stagnation point over a stretching cylinder increases both the skin friction coefficient and the surface heat transfer rate. Wu et al. [8], considered displacement thickness as the thickness of the liquid film in an ideal annular flow. The boundary layer, affected by the Reynolds number, experiences changes in thickness and behavior. Higher Reynolds numbers result in a larger, more turbulent boundary layer, leading to increased drag.

Research Progress in Mechanical and Manufacturing Engineering Vol. 5 No. 1 (2024) p. 662-671

The Reynolds number affects a car's drag coefficient C_D, representing its aerodynamic resistance. As the Reynolds number increases, the drag coefficient decreases and stabilizes [9]. According to El Hasadi & Padding [10], the drag coefficient of a sphere is influenced by the Reynolds number. At higher Reynolds numbers, the drag coefficient tends to increase due to increased flow separation, larger wake regions, and turbulent flow effects. Mallick [11], that the drag coefficient variation on rough cylindrical bodies is influenced by the Reynolds number, which measures aerodynamic resistance. Consequently, the Reynolds number does impact a car's drag coefficient. Flow separation occurs when a fluid's boundary layer breaks away from the solid boundary, typically where it diverges from the mean flow direction. Based on the research by Kourta & Gillieron [12], there are various solutions to control separation and reduce aerodynamic drag, including active flow control by fluidic actuators and passive control systems using obstacles. According to Southard [13], the occurrence of flow separation depends significantly on the boundary's orientation relative to the overall flow. The boundary's orientation affects fluid flow, potentially causing turbulence or separation.

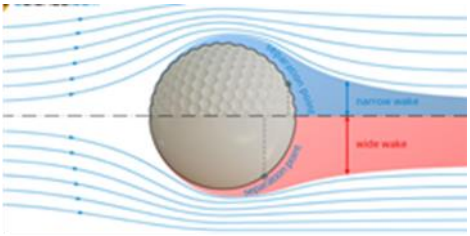

Fig. 1 *Dimples on a golf ball to create a turbulent flow around it*

Lift force acts perpendicular to the motion and results from pressure differences on a vehicle's upper and lower surfaces as it moves through air. Positive lift is undesirable as it reduces tire grip, while negative lift (downforce) enhances road holding [14]. Nath et al. [15] discusses the effects of different aerodynamic devices on lift force. The results shows that lift force increases exponentially with the increase in speed. Drag force is a major setback when it comes to achieving high speeds in a moving vehicle. Velagapudi et al. [16], improve the geometry of the car for a better flow around the model and a lower drag coefficient. The analysis demonstrates that the aerodynamic drag for a car body increases equal to the square of velocity in terms of drag forces or drag coefficient. Barnard et al. [17] addressed challenges in reducing aerodynamic drag in large goods vehicles (LGVs), highlighting box designs causing pressure drag and separation. Based on research by Mukut & Abedin [18], a dramatic increase in drag at high speeds, constituting 70% of the whole vehicle resistance. According to Nath et al. [15], improved aerodynamics of a vehicle can provide several benefits such as reduction in drag force, which can help achieve higher speeds and improve fuel economy.

The aerodynamic drag problem is always influenced by the geometry of a car's body. The drag, which plays a significant role in the resistance experienced by vehicles, becomes particularly prominent at higher speeds. When it comes to two-seater sports cars, the design of the body shape becomes even more crucial in minimizing drag and optimizing performance during motion. Analyzing the aerodynamics of two-seater cars with ANSYS CFX software is crucial for understanding how velocity influences performance. This examination helps optimize designs, reduce aerodynamic drag, and improve fuel efficiency, contributing to enhanced acceleration, top speed, maneuverability, and overall effectiveness of the vehicle. Thus, this study will aim to investigate the flow characteristic over two-seater car, to evaluate the aerodynamic performance of two-seater car and to compare the aerodynamic performance between different two-seater cars.

2. Methodology

This research involves using a car body designed in SOLIDWORKS as the test panel to gather data. The study includes conducting tests at three different velocities (20 m/s, 30 m/s, and 50 m/s) for four types of models. The data collection is based on the solution of Fluid Flow (Fluent). To ensure the accuracy, reliability, and validity of the acquired data, the data collection procedure must be meticulously planned and executed.

2.1 Computational Method

In this study, the Nissan Skyline, Porsche 918 Spyder, Bugatti Chiron and Ford Mustang are chosen as car models. All types of two-seater car have the same design as the real car model and the designs were in minimum of precision geometries. Fig. 2 depicts the model car's relative to their actual size.

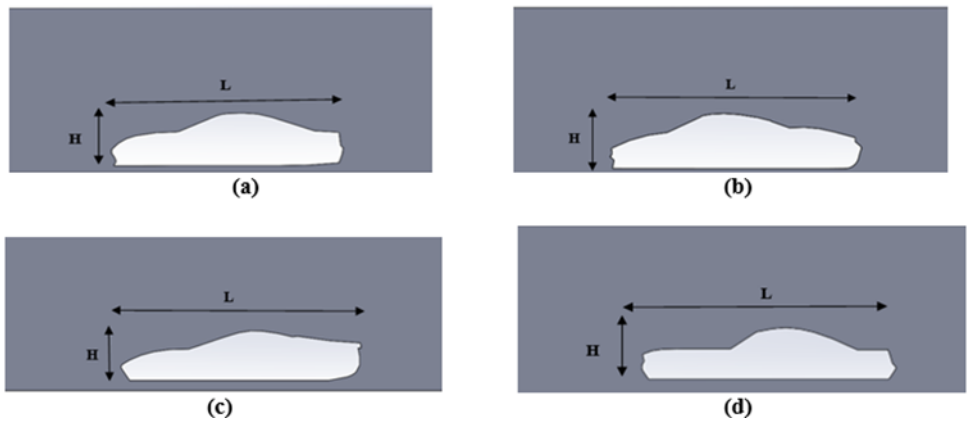

Fig. 2 *Geometry detail from side view of (a) Nissan Skyline (b) Porsche 918 Spyder (c) Bugatti Chiron (d) Ford Mustang*

As outlined in the preceding chapter on the scope of the study, certain limitations have been imposed for the sake of study simplicity. Notably, the model does not encompass elements such as windows, mirrors, lights, and doors. Table 1 shows the Geometric configuration of the car models.

Table 1 *Geometric configuration of the car models*

Geometric configuration of the car	Dimension of the car model (mm)			
	Nissan Skyline	Porsche 918 Spyder	Bugatti Chiron	Ford Mustang
Length of the car model, L	4594.82	4127.49	5382.90	5043.53
Height of the car model, H	1182.50	926.46	1520.20	1098.31

The dimensions where the modelling of fluid flow or other physical processes occurs is referred to as the computational domain dimension in numerical simulations. In applications like CFD simulations of aerodynamics, the computational domain must be appropriately sized to encompass relevant flow patterns and interactions with the studied geometry. Fig. 3 depicts the computational domain dimension for all car models.

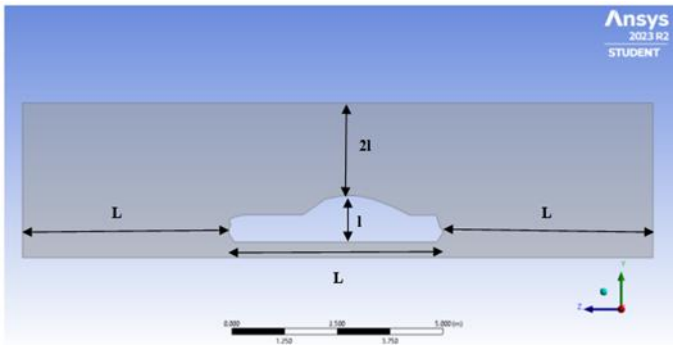

Fig. 3 *Computational domain dimension for car models*

L = Length of the car model
l = Height of the car model

Boundary conditions establish the parameters for how air interacts with a vehicle in simulations or experiments. These conditions dictate the flow characteristics and simulate real-world aerodynamic scenarios, ensuring that the results align with the physical behavior of air around the car.

Research Progress in Mechanical and Manufacturing Engineering Vol. 5 No. 1 (2024) p. 662-671

Table 2 *Boundary conditions for all car models*

Boundary	Boundary Types	Values
Inlet	Velocity inlet	20m/s, 30m/s and 50m/s
Outlet	Pressure outlet	0 Pa
Top	Symmetry	-
Side	Symmetry	-
Bottom	Stationary wall	-
Car body	Stationary wall	-

2.2 Meshing

The process of meshing is the dividing of a geometric model into distinct parts or cells. In the ANSYS simulation environment, a mesh is a computational grid that reflects the geometry of the product being analyzed, such as a part or an assembly.

2.2.1 Mesh Dependency Test

In ANSYS, a numerical analysis method used in computational fluid dynamics simulations is known as a mesh dependency test. Finding the best mesh resolution to produce precise and reliable results in ANSYS simulations and building reliance on the numerical model both depend on the grid dependency test. Based on Fig. 4, the simulation runs with element sizes of 0.02,0.03, and 0.05 with the car model Porsche 918 Spyder at an inlet velocity of 20m/s. Finer mesh, or smaller elements, often yields more accurate results, especially when it comes to capturing localized variations and gradients inside the structure.

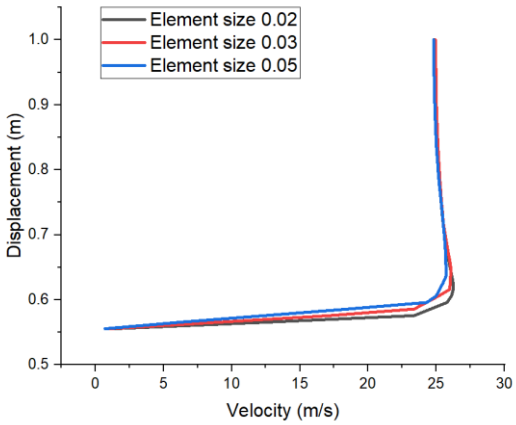

Fig. 4 *Graph for Mesh Dependency Test*

The recorded maximum velocities for varying element sizes (0.02, 0.03, and 0.05) in the context of our simulation are 26.23 m/s, 26.07 m/s, and 25.71 m/s, respectively. To assess the differences among these element sizes, percentage differences were calculated with element size 0.02 as the reference point. The results indicate that the percentage difference between element size 0.05 and 0.02 is 1.97%, whereas the percentage difference between element size 0.03 and 0.02 is 0.59%. As conclusion, it has been concluded to utilize element size 0.03 for running simulations across all car models, given its representation of the physical behavior with the lowest percentage difference observed among the tested element sizes.

2.2.2 Validation of the Study

In order to validate the created computational model and the utilized geometrical discretization, a simulation was performed using the widely employed generic Ahmed body, similar to the car models that were used in this study. The dimensions of the Ahmed body are illustrated in Fig. 5.

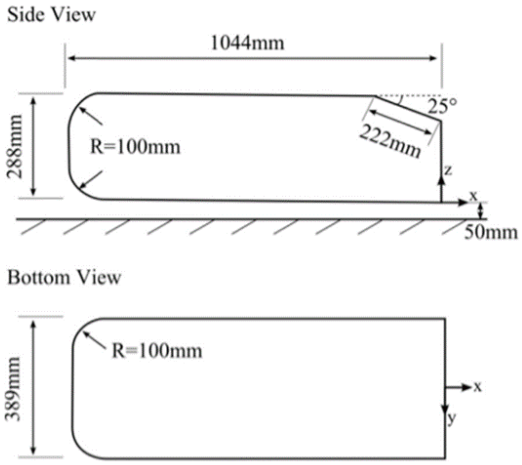

Fig. 5 *Dimensions of Ahmed body*[19]

Numerical investigations on the Ahmed body were conducted by M. Bambhania et al. and M. Govardhana. They opted for a three-dimensional Ahmed body model in their numerical simulation work. In the current study, an effort has been made to attain results using a two-dimensional computational model for numerical simulation, aiming to decrease computational time. Results were generated for a velocity of 40 m/s with zero outlet gauge pressure.

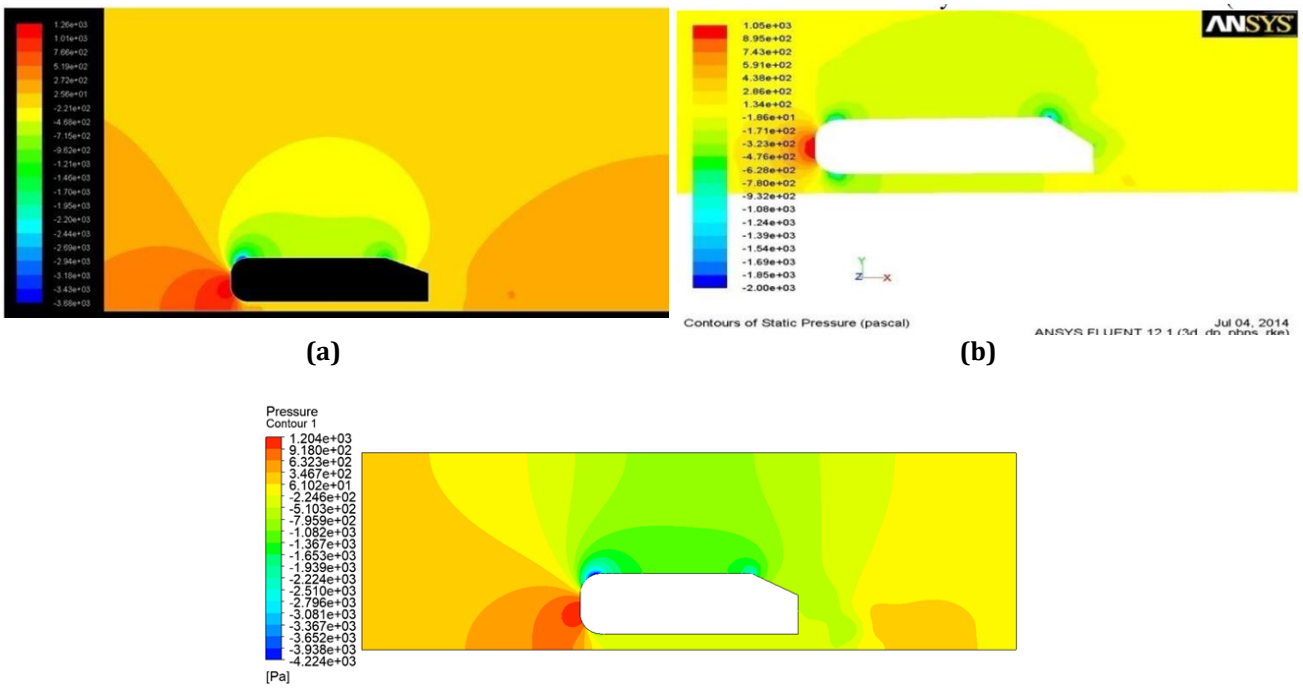

(a) **(b)**

(c)

Fig. 6 *Pressure contour (a) by M.Bambhania et. al.*[19] *(b) by M. Govardhana et. al.*[20] *(c) in present study*

Based on Fig. 6, the different coloured zones indicate different values of pressure. The maximum pressure field is highest at the front portion of the body for all three simulations.

Table 4 Result obtained for validation

Numerical Simulation	Maximum pressure, Pa
Simulation by M.Bambhania et. al	1200
Simulation by M.Govardhana et. al.	1050
Simulation in present study	1204

Research Progress in Mechanical and Manufacturing Engineering Vol. 5 No. 1 (2024) p. 662-671

The conclusion achieved by comparing the maximum pressure of all three simulations is clearly shown in Table 4. In conclusion, there is a good agreement between the results of 3D and 2D computational models in simulations.

3. Result and Discussion

This chapter will discuss about flow characteristics and pressure coefficients of Nissan Skyline, Porsche 918 Spyder, Bugatti Chiron and Ford Mustang.

3.1 Flow Characteristic

In this ANSYS simulation, the flow characteristics were analysed around a two-seater car to gain insights into its aerodynamic performance. The simulation focus on velocity contours, pressure distribution, and streamlines.

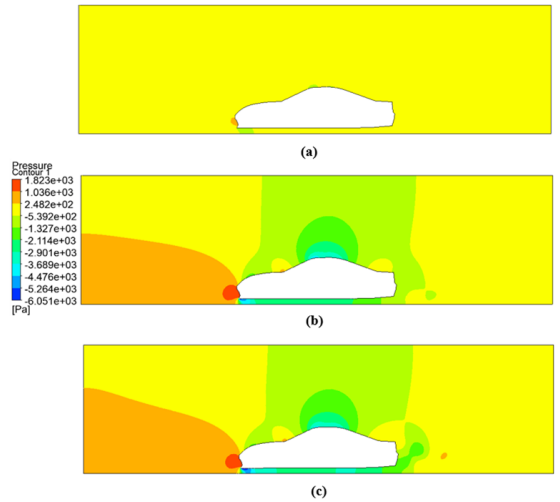

Fig. 7 *Pressure distribution of car model Nissan Skyline (a) Velocity 20m/s (b) Velocity 30m/s (c) Velocity 50m/s*

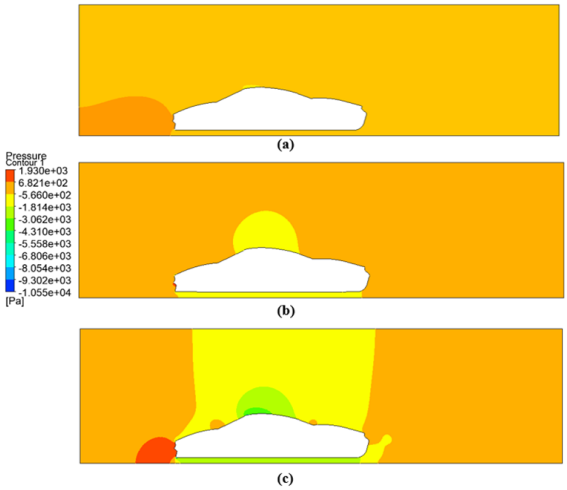

Fig. 8 *Pressure distribution of car model Porsche 918 Spyder (a) Velocity 20m/s (b) Velocity 30m/s (c) Velocity 50m/s*

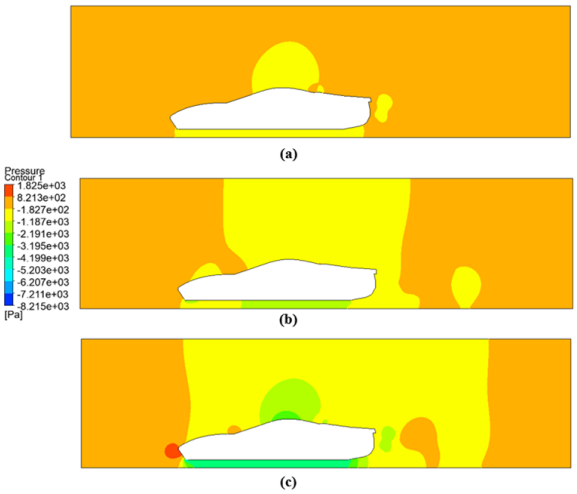

Fig. 9 *Pressure distribution of car model Bugatti Chiron (a) Velocity 20m/s (b) Velocity 30m/s (c) Velocity 50m/s*

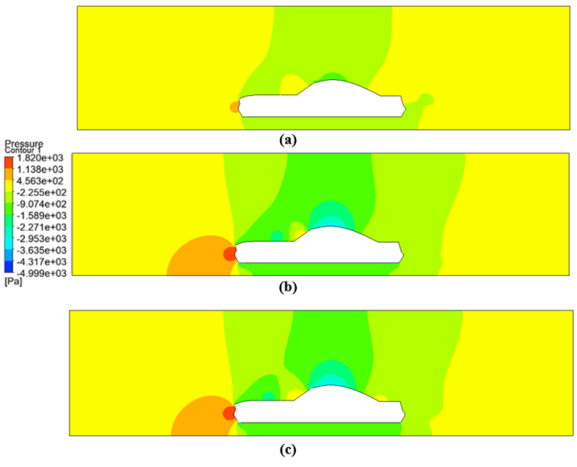

Fig. 10 *Pressure distribution of car model Ford Mustang (a) Velocity 20m/s (b) Velocity 30m/s (c) Velocity 50m/s*

Based on Fig. 7, Fig. 8, Fig. 9 and Fig. 10, Nissan Skyline exhibits high pressure at its front, recording a maximum of 1823.01 Pa, signaling increased air resistance. Conversely, the minimum pressure occurs on the upper surfaces at -6051.08 Pa, contributing to lift forces. In contrast, the Porsche 918 Spyder displays high-pressure zones at the front, with the highest pressure recorded at 1930.08 Pa for velocities of 30 m/s and 50 m/s. The Bugatti Chiron demonstrates varying pressure levels, with the highest pressure at 50 m/s, ranging from 1825 Pa to -6207 Pa. The Ford Mustang, characterized by increased pressure at the front for aerodynamic efficiency, exhibits the lowest overall pressure at 20 m/s, ranging from –907.4 Pa to 1138 Pa, and the highest

pressure at 50 m/s. In summary, the Porsche 918 Spyder and Bugatti Chiron tend to have higher pressures at the front compared to the Nissan Skyline and Ford Mustang, with each model displaying unique pressure characteristics influenced by their design and velocity.

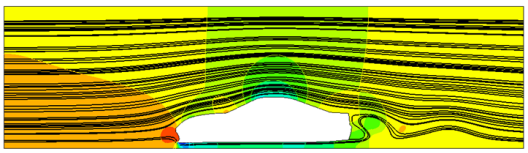

Fig. 11 *Streamline along car model Nissan Skyline*

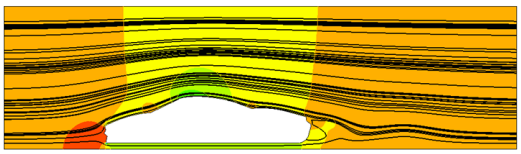

Fig. 12 *Streamline along car model Porsche 918 Spyder*

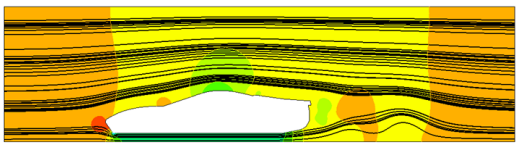

Fig. 13 *Streamline along car model Bugatti Chiron*

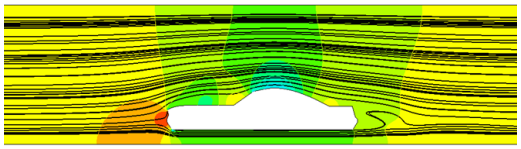

Fig. 14 *Streamline along car model Ford Mustang*

According to Fig. 11, Fig. 12, Fig. 13 and Fig. 14, the streamline analyses of the Nissan Skyline, Porsche 918 Spyder, Bugatti Chiron, and Ford Mustang reveal distinctive aerodynamic profiles and airflow characteristics. The Nissan Skyline demonstrates a convergence of streamlines along the hood and windshield, aligning with Bernoulli's principle and highlighting the aerodynamic wake for in-depth analysis of drag and lift forces. In the case of the Porsche 918 Spyder, smoothly curved streamlines over the hood and roof showcase a well-designed aerodynamic profile that minimizes turbulence. The Bugatti Chiron's study emphasizes smoothly curved streamlines over the hood, successful avoidance of turbulence, and divergence towards the back, indicating efficient aerodynamic design. Lastly, the Ford Mustang's streamline analysis reveals a design facilitating efficient airflow with curved streamlines along the hood, convergence towards the windshield, and splitting near the rear. Each car's unique characteristics provide valuable insights into their respective aerodynamic efficiency and performance attributes.

3.2 Pressure Coefficient, C_p

Fig. 15, Fig. 16, Fig. 17 and Fig. 18 show the pressure coefficient (Cp) plotted against distance (Z) for three distinct velocities: 20 m/s, 30 m/s, and 50 m/s.

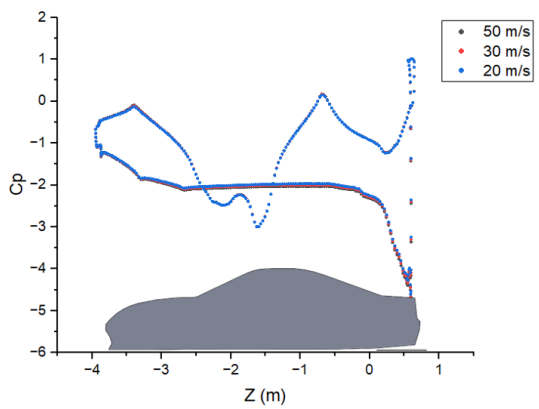

Fig.15 *Pressure coefficient, C_P along the car Z-axis for Nissan Skyline*

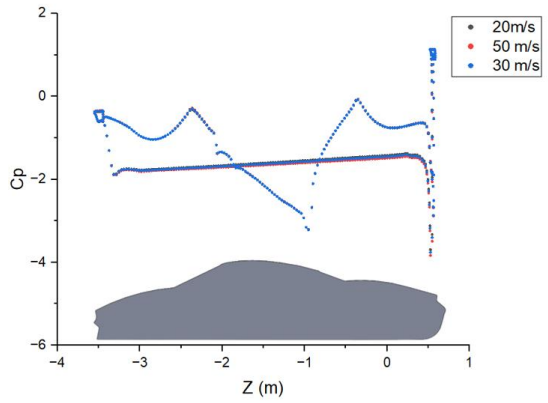

Fig. 16 *Pressure coefficient, C_P along the car Z-axis for Porsche 918 Spyder*

Research Progress in Mechanical and Manufacturing Engineering Vol. 5 No. 1 (2024) p. 662-671

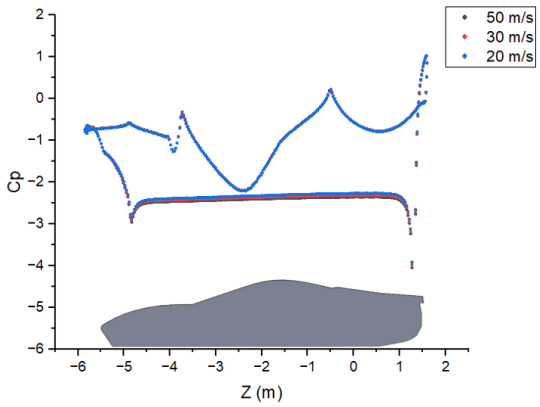

Fig. 17 *Pressure coefficient, C_P along the car Z-axis for Bugatti Chiron*

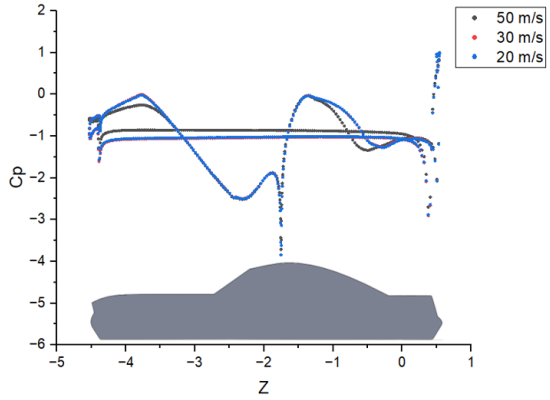

Fig. 18 *Pressure coefficient, C_P along the car Z-axis for Ford Mustang*

A positive Cp denotes a pressure at a point higher than the free-stream pressure, while a negative Cp signifies a pressure lower than the free-stream pressure. The graphs consistently depict negative Cp values across all distances from the body for all three velocities, indicating that the pressure on the body's surface is consistently lower than the free-stream pressure. The Cp values are also generally more negative at higher velocities. This is because the faster the air flows over the body, the greater the pressure difference between the top and bottom surfaces of the body. From the figures, the highest Cp value for the Ford Mustang is at 50 m/s, while the Nissan Skyline, Porsche 918 Spyder, and Bugatti Chiron have the highest Cp at a velocity of 20 m/s.

4. Conclusion and Recommendation

In conclusion, the flow characteristics and aerodynamic performance of a two-seater car have been successfully carried out. The outcomes derived through the utilization of Computational Fluid Dynamics (CFD) software are thoroughly deliberated in Chapter 4. The Bugatti Chiron exhibits the highest pressure. At a velocity of 50 m/s, the pressure recorded on the Bugatti Chiron ranges from 1825 Pa to -6207 Pa. Meanwhile, the Ford Mustang has the lowest overall pressure among the analyzed car models. At a velocity of 20 m/s, the pressure on the Ford Mustang ranges from –907.4 Pa to 1138 Pa. Higher pressure is observed at the front for all car models and lowest at the upper car surface. The investigation proves the inverse relationship between pressure and velocity, confirming that an increase in velocity corresponds to a decrease in pressure in the respective area. Streamline analyses of the Nissan Skyline reveal convergence along the hood and windshield, indicating aerodynamic efficiency. The Porsche 918 Spyder displays smoothly curved streamlines over the hood, minimizing turbulence for an efficient design. The Bugatti Chiron's study emphasizes streamlined efficiency over the hood and successful turbulence avoidance. The Ford Mustang's analysis indicates an airflow-efficient design with curved streamlines and convergence towards the windshield. Graphs of pressure coefficient consistently show negative Cp across all distances for all velocities, indicating lower pressure on the body's surface. The highest Cp value for Ford Mustang is at 50 m/s while Nissan Skyline, Porsche 918 Spyder and Bugatti Chiron has the highest Cp at velocity 20 m/s. Based on the results, Nissan Skyline, Porsche 918 Spyder and Bugatti Chiron tend to have consistently low average Cp values, suggesting potentially better aerodynamic efficiency.

There are few problems and limitations appear while using Ansys CFX (Student Version). ANSYS Student versions often come with inherent limitations, such as constraints on problem size, including restrictions on nodes, elements, and degrees of freedom in simulations. The absence of technical support necessitates users to rely on online forums and community discussions for guidance. To address these limitations, strategies were recommended like dividing complex simulations to fit within the node and element limitations. Consider simplifying geometries or using symmetry to reduce the problem size. Moreover, students can collaborate with educational institutions for access to the commercial version while seeking assistance from supervisors or online communities for technical challenges.

Acknowledgement

The authors would like to thank the Faculty of Mechanical and Manufacturing Engineering, University Tun Hussein Onn Malaysia for its support.

References

[1] Y. Sun, Q. Liu, L. Shao, Y. Wang, X. Chang, and K. Liu, "Experimental investigation of aerodynamic forces and vortex-induced vibrations of wavy cylinders at subcritical Reynolds numbers," *Exp. Therm. Fluid Sci.*, vol. 144, no. September 2022, p. 110869, 2023, doi: 10.1016/j.expthermflusci.2023.110869.

[2] G. K. Ananda, P. P. Sukumar, and M. S. Selig, "Measured aerodynamic characteristics of wings at low Reynolds numbers," *Aerosp. Sci. Technol.*, vol. 42, pp. 392–406, 2015, doi: 10.1016/j.ast.2014.11.016.

[3] S. Kumahor and M. F. Tachie, "Turbulent flow around a short rectangular cylinder in uniform flow at moderate Reynolds numbers," *Exp. Therm. Fluid Sci.*, vol. 147, no. March, p. 110960, 2023, doi: 10.1016/j.expthermflusci.2023.110960.

[4] Anup Kumar Dey, "What is the Reynolds Number? The Equation for Reynolds Number and its Significance," What is Piping. Accessed: Jun. 17, 2023. [Online]. Available: https://whatispiping.com/reynolds-number/

[5] X. Luo, W. Zhang, H. Dong, A. K. Thakur, B. Yang, and W. Zhao, "Numerical analysis of heat transfer enhancement of fluid past an oscillating circular cylinder in laminar flow regime," *Prog. Nucl. Energy*, vol. 139, no. March, p. 103853, 2021, doi: 10.1016/j.pnucene.2021.103853.

[6] A. G. Weiss, P. J. Kristo, J. R. Gonzalez, and M. L. Kimber, "Flow regime and Reynolds number variation effects on the mixing behavior of parallel flows," *Exp. Therm. Fluid Sci.*, vol. 134, no. December 2021, p. 110619, 2022, doi: 10.1016/j.expthermflusci.2022.110619.

[7] T. Salahuddin, M. Y. Malik, A. Hussain, M. Awais, I. Khan, and M. Khan, "Analysis of tangent hyperbolic nanofluid impinging on a stretching cylinder near the stagnation point," *Results Phys.*, vol. 7, pp. 426–434, 2017, doi: 10.1016/j.rinp.2016.12.033.

[8] H. Wu, Y. Xu, X. Xiong, E. Mamat, J. Wang, and T. Zhang, "Prediction of pressure drop in Venturi based on drift-flux model and boundary layer theory," *Flow Meas. Instrum.*, vol. 71, no. August 2019, p. 101673, 2020, doi: 10.1016/j.flowmeasinst.2019.101673.

[9] K. Ngo, Chean Chin , Gramoll, *Fluid Mechanics - Theory*. Kurt Gramoll, 2021. [Online]. Available: https://www.ecourses.ou.edu/cgi-bin/ebook.cgi?chap_sec=09.1&page=theory&topic=fl

[10] Y. M. F. El Hasadi and J. T. Padding, "Do logarithmic terms exist in the drag coefficient of a single sphere at high Reynolds numbers?," *Chem. Eng. Sci.*, vol. 265, p. 118195, 2023, doi: 10.1016/j.ces.2022.118195.

[11] M. Mallick, "Variation Of Drag Coefficient A Dissertation Submitted in Partial Fulfillment of the Requirements," no. May, p. 84, 2014, doi: 10.13140/RG.2.1.3202.3926.

[12] A. Kourta and P. Gilliéron, "Impact of the automotive aerodynamic control on the economic issues," *J. Appl. Fluid Mech.*, vol. 2, no. 2, pp. 69–75, 2009, doi: 10.36884/jafm.2.02.11871.

[13] J. B. Southard, "Introduction to Fluid Motions and Sediment Transport," *Book*, p. 369, 2019.

[14] H. Heisler, "Vehicle body aerodynamics," *Adv. Veh. Technol.*, pp. 584–634, 2002, doi: 10.1016/b978-075065131-8/50015-4.

[15] D. S. Nath, P. C. Pujari, A. Jain, and V. Rastogi, "Drag reduction by application of aerodynamic devices in a race car," *Adv. Aerodyn.*, vol. 3, no. 1, 2021, doi: 10.1186/s42774-020-00054-7.

[16] N. K. Velagapudi, L. N. K., L. N. V. N. Rao, and S. R. Y., "Investigation of Drag and Lift Forces over the Profile of Car with Rearspoiler using CFD," *Int. J. Adv. Sci. Res.*, vol. 1, no. 8, p. 331, 2015, doi: 10.7439/ijasr.v1i8.2510.

[17] A. R. Barnard, Z. Wang, and Y. M. Chung, *Drag-reduction devices to improve the aerodynamic efficiency of close-coupled large goods vehicles*. Woodhead Publishing Limited, 2014. doi: 10.1533/9780081002452.7.239.

[18] A. N. M. M. I. Mukut and M. Z. Abedin, "Review on Aerodynamic Drag Reduction of Vehicles," *Int. J. Eng.*

Mater. Manuf., vol. 4, no. 1, pp. 1–14, 2019, doi: 10.26776/ijemm.04.01.2019.01.

[19] M. P. Bambhania and J. Deepak, "Numerical Simulation Of Two-Dimensional Ahmed Body Numerical Simulation Of Two-Dimensional Ahmed Body Abstract :," no. March, 2016, doi: 10.13140/RG.2.1.1813.9285.

[20] M. Govardhana and D. B. V. Reddy, "Estimation of Drag and Lift on Ahmed Body Using CFD Analysis," *Int. J. Adv. Innov. Res.*, vol. 3, no. 8, pp. 51–55, 2017.